Computers and Structures 162 (2016) 91–101

Contents lists available at ScienceDirect

Computers and Structures

journal homepage: www.elsevier.com/locate/compstruc

An irregular lattice model to simulate crack paths in bonded granular assemblies

Christine Myra Sands

School of Engineering, King's College, University of Aberdeen, Aberdeen AB24 3UE, United Kingdom

ARTICLE INFO

Article history:
Received 2 July 2014
Accepted 22 September 2015
Available online 24 October 2015

Keywords:
Granular
Lattice
Inter-granule bonds
Lattice model

ABSTRACT

A 2D model of a bonded granular material is presented and its properties confirmed to be that of a brittle, isotropic elastic solid. The bond stiffnesses (axial tension/compression, shear and bending) are taken from the classical solutions to the external crack problem with two half-spaces bonded by a disc of intact material. An assembly of granules is simulated using a random array of points (representing the granule locations) with a prescribed minimum separation. The bonds are then generated by a Delaunay triangulation. This produces an isotropic array of bonds giving rise to a model material with isotropic properties. Crack growth is simulated by sequentially removing the most highly stressed bond in turn. Crack paths are then produced which are shown to agree with the predictions of linear elastic fracture mechanics, in respect of both the direction of propagation and the influence of specimen size. Some well-known problems are then simulated including: the interaction of two parallel cracks; diametrical compression of a disc; the four point bending of a beam; the influence of mortar strength on the behaviour of masonry; and a flat arch.

1. Introduction

This paper focuses on a model developed to simulate the response of granular assemblies to mechanically induced stress. The granules are bonded only where they are in contact, and the bond strength is significantly less than the granule strength. As such it can clearly be used to simulate the behaviour of many sedimentary rocks and a wide variety of ceramic materials, including some cement bonded blocks and many refractory products. The lattice model presented is, in effect, a sheet of three dimensional granules with all the bonds in the plane of the model. Consequently the model is currently only two dimensional; but the techniques used could easily be extended to three dimensions.

Lattice models have proved popular and have been used to simulate the behaviour of particulate materials generally [1–4]; rocks [5–8], and even a much wider range of brittle materials (e.g. concrete [9–13]) that do not have a microstructure that directly corresponds to the bonded granule idealisation.

Models of granular assemblies generally consist of:

- an assembly of granules with a lattice of bonds between (or near) the contacts;
- a prescription of bond stiffnesses;
- a prescription of bond strengths.

An assembly of granules and connecting bonds can be defined in a model in a number of different ways. Chandler [14] used a 2D hexagonal lattice of equally sized bonded spheres and created initial structural irregularities by randomly assigning some bonds to be missing. More recently, the positions, shape and orientation of granules in the model material are commonly distributed randomly and arbitrarily, but a real material can be measured and then reproduced in the model [2,5]. This approach has become more popular as computerised tomography has become more widely available. While many two dimensional models have been used successfully, three dimensional lattice models have also been developed [15,16].

Regular lattices in which all the elements have the same linear elastic properties have been shown to simulate linear elastic behaviour in the bulk material, however it has been shown [17,9] that the crack pattern produced depends very significantly on the lattice layout. A random lattice produces a more realistic result that appears to be independent of the particular lattice, but uniform material response commonly requires the properties of the elements to be adjusted to ensure that uniform strain results in uniform stress within the lattice. While that may present a problem for modelling perfectly homogeneous materials, it may not be an issue with materials that, while homogeneous at a large scale, are not so at the scale of the lattice.

Many models simulate the bonds between the nodes of the lattice (regarded as the locations of the granules in the model

E-mail address: c.sands@abdn.ac.uk

http://dx.doi.org/10.1016/j.compstruc.2015.09.006
0045-7949/

presented here) as springs [18,6,7,15], but beam theory is also used [1,19,20]. While most lattice models are based on linear elasticity, some have used viscous, cohesive crack, crack bridging, tension softening and other non-linear approaches [21–24] and some incorporate post-fracture compressive and frictional interaction [25–27]. While most lattice models use failure criteria based on stress, strain based systems have been used [19].

Lattice-like models using discrete element methods (DEM) have also been widely used [28,8,29–31] and although they have generally been limited to considering spherical or ellipsoidal granules, the bond stiffnesses are often similar to those used in more obviously lattice models. Discrete element methods also have the advantage that new contacts can be formed, and previously fractured bonds re-formed, that can pass shear and compression (though not tension) between granules.

Several continuum models [32–35] that can simulate crack growth in brittle materials have been developed based on a damage mechanics approach. Usually the stress and strain within the body is computed based on linear elastic theory and a threshold is set for the onset of damage. The elastic modulus is then permitted to degrade in accordance with a rule, or rules, that may be based on some mechanistic concept [32], be guided by empirical work [33], or by a widely accepted geomechanical model [34], or simply follow a realistic tension softening profile [35]. Although such models have advantages, such as the ease with which they can be incorporated into finite element analysis, they cannot capture the material behaviour at a fine scale. Lattice-particulate models, of the type presented in this paper, have an advantage in that respect.

The model presented in this paper is based on the linear elastic theory for the bending, tension and shear of two half-spaces; and bond failure is assumed to occur in pure tension. It focusses on simulating crack path development by sequentially breaking (and then removing from consideration) the most severely stressed bond. This is done one bond at a time, permitting stable crack growth to be simulated and also unstable crack growth in situations where inertial effects are negligible. The crack paths produced have been compared with recognised criteria [36] and observations [37–39]. Finally the model is used to explore qualitatively the influence of mortar strength on the performance of structural masonry. In these simulations the model is used for the purposes of comparison only and the simulations do not relate to any specific material. It follows that any numerical values provided in respect of, for example, loads or displacements are not significant.

A variety of different models have been used to simulate the response of masonry to applied load or foundation movement. Vertical loads were traditionally handled by considering the masonry as a no-tension structure and ensuring stability while avoiding local crushing of the material. More modern approaches take account of the bonding effect of the mortar joints. Pande et al. [40], developed a procedure to establish orthotropic material properties for masonry panels which was then applied that to finite element analysis modified by a smeared crack approach [41]. Alpa and Monetto [42] applied theories relating to the frictional response of arrays of microcracks and considered walls with in-plane loading, while Anthoine [43] used the theory of periodic media to establish homogenised properties. Luciano and Sacco [44] used a representative volume based on a masonry unit with adjoining mortar and considered the possible crack paths that could form and the consequent states of the masonry to determine characteristic moduli for each state. Homogenization techniques were then adopted to establish a nonlinear constitutive law for the masonry material.

A common approach for thin walls subjected to lateral loads treats masonry panels as plates [45–47], and that approach can be extended to include vertical loads [48]. Another technique [49,50] uses discrete element methods, often supported by homogenization techniques and the use of representative volumes. While these approaches have several advantages, they lack the simplicity of the model presented here.

2. Construction of the lattice

2.1. The nodes and bonds

In the model presented here, random points are generated in succession and discarded if a new point falls outside a defined area or is too close to any other existing point. In this way an irregular, but reasonably evenly distributed, set of points is created. Each of these points represents the location of the centroid of a granule and forms a node in the lattice. Each node can translate in two dimensions and rotate. A Delaunay triangulation is then performed to define which nodes are connected to a neighbouring node. Each bond connects two nodes and the granule to granule bond is assumed to exist halfway between the two connected nodes. The model, therefore, models non-spherical granules.

Fig. 1 illustrates a typical granular structure of the sort being simulated in the work presented here, overlain by the lattice structure used to simulate the granular assembly. The blue dots are nodes in the lattice and each node represents the centroid of a grain. The bonds between the grains are represented by the lattice members (shown as red lines) and the contacts between the grains are assumed to act at the mid-point of the lattice member. In the simulations presented in this paper the area of the bond connecting two grains was, on average, about 1.5% of the surface area of each of the grains that the bond connected, with a maximum of 3.7%; justifying the assumption that the contact area was small. The diameter of the grains was, on average, about 1.2% of the size of the body being simulated.

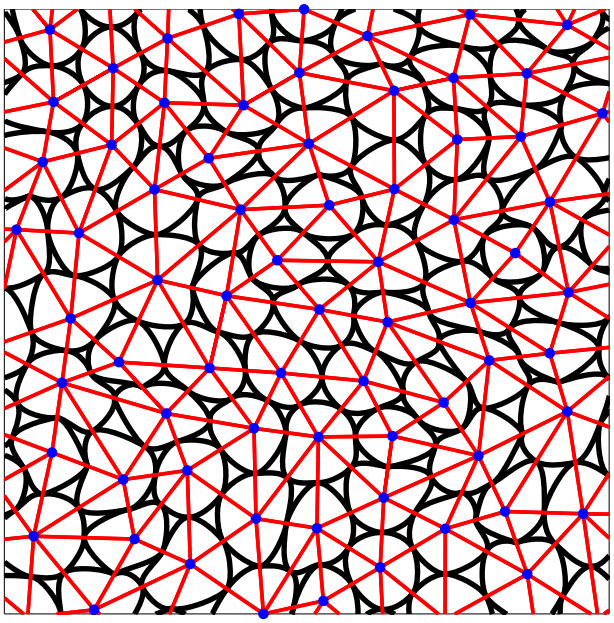

Fig. 1. A typical granular assembly (shown as black lines) with the structure of the model representing the assembly superimposed. The nodes that represent the grains are shown as blue dots, and the lattice members that encapsulate the bonds are shown as red lines. The nodes act at the centroid of the grains and the contacts are taken as acting at the mid-point of the lattice members that connect the nodes. (For interpretation of the references to colour in this figure legend, the reader is referred to the web version of this article.)

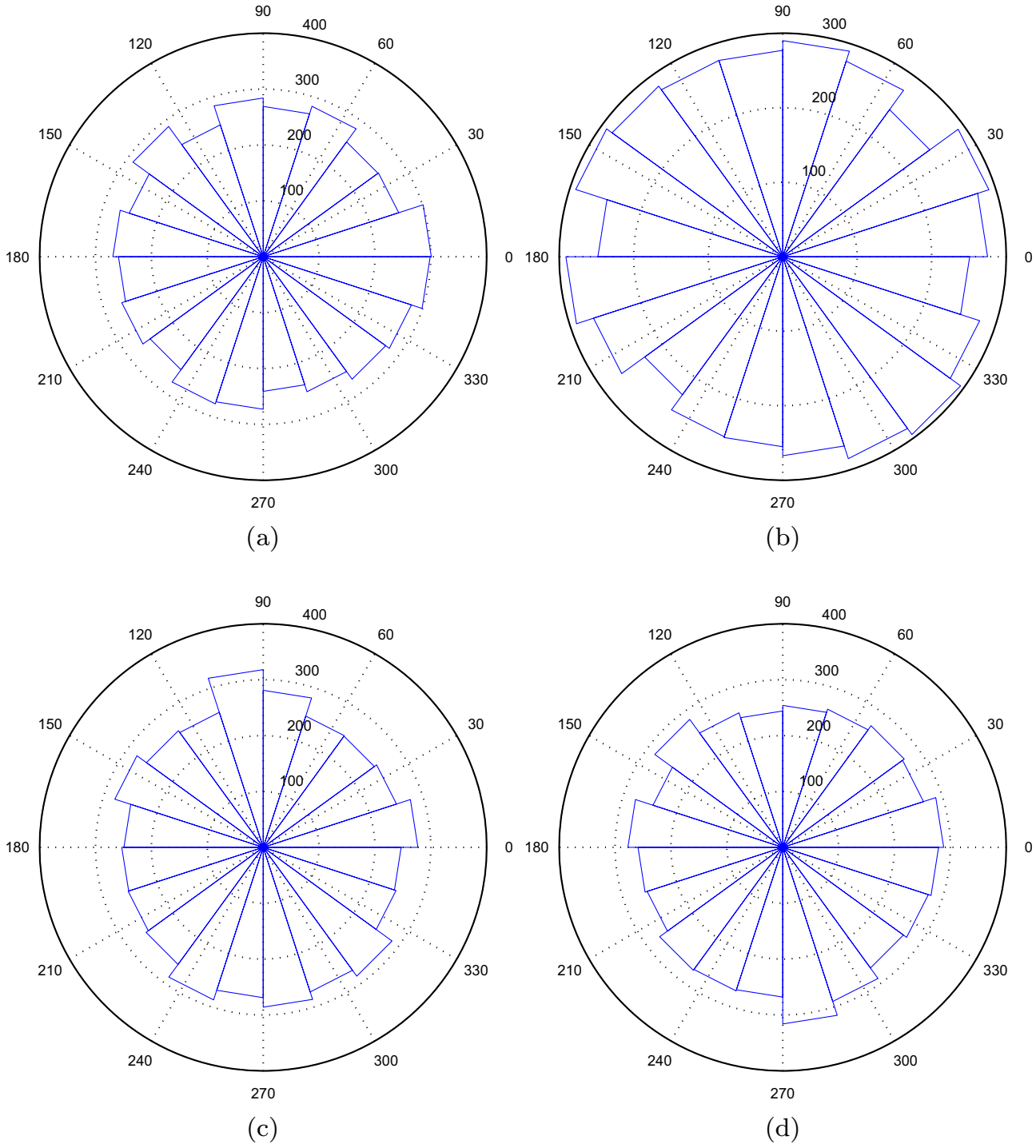

Fig. 2. Polar histograms of bond orientations.

2.2. The bond stiffness

The area of each bond is assumed to be small in comparison to the surface area of the granules. The bond stiffnesses (axial tension/compression, shear and bending) are taken from the classical solutions to the external crack problem with two half-spaces bonded by a disc of intact material. Barber [51] gives expressions for the case of the related problem of a cylindrical rigid punch of radius a that is pushed, by a normal compressive force $-t$, a distance $-e_x/2$ into an elastic half space that has shear modulus G and Poisson's ratio v.

$$t = \frac{4Ga\left(\frac{e_x}{2}\right)}{(1-v)}. \tag{1}$$

Bending stiffness is found by considering the case of a punch that is tilted through an angle $\phi/2$ by a moment m such that

$$m = \frac{8Ga^3\left(\frac{\phi}{2}\right)}{3(1-v)}. \tag{2}$$

Shear stiffness is found (using Johnson [52]) by considering the tangential force q required to produce a tangential displacement, $e_y/2$, of a granule

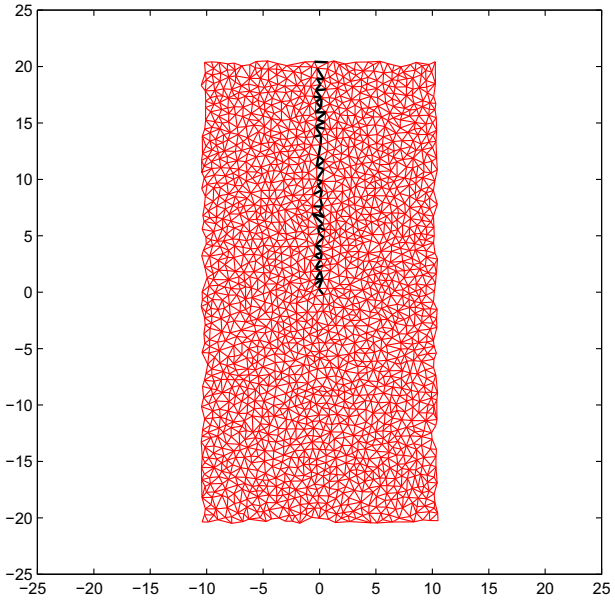

Fig. 3. Rectangular test sample with pre-crack shown as thick black lines.

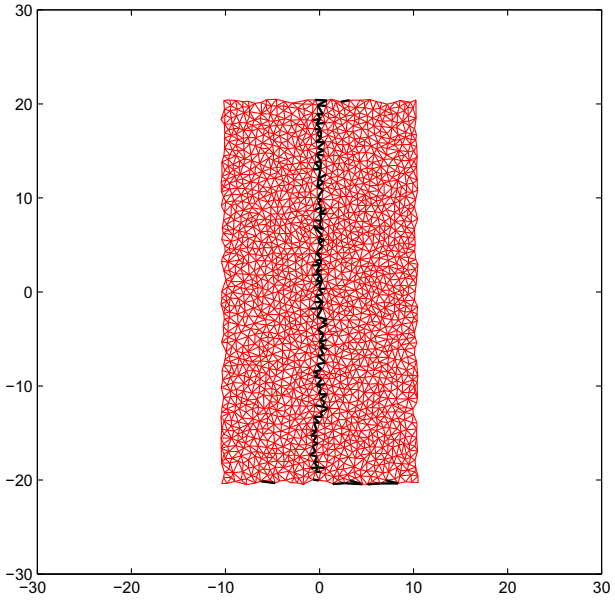

Fig. 4. Rectangular test sample after crack extension. Cracks shown as thick black lines.

$$q = \frac{4Ga}{(2-\nu)}\left(\frac{e_y}{2}\right). \tag{3}$$

The stiffnesses presented above can be written, for the combined deformation of the two half-spaces, in terms of Young's modulus (E) and Poisson's ratio (ν) as follows

$$\frac{Ea}{(1-\nu^2)}, \tag{4}$$

for the axial case,

$$\frac{2Ea}{((2-\nu)(1+\nu))}, \tag{5}$$

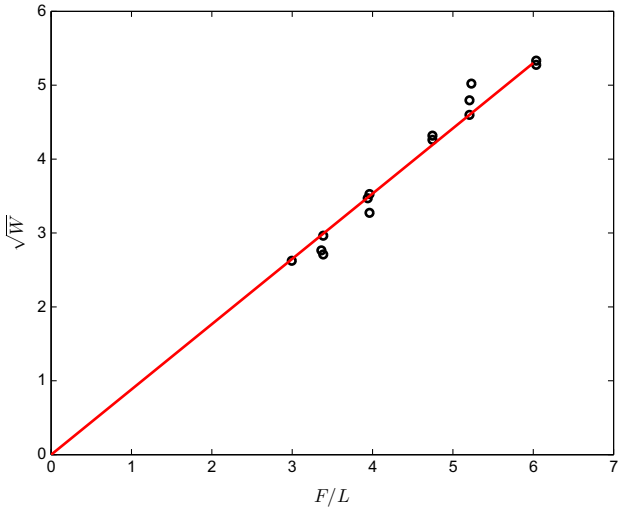

Fig. 5. Confirmation of the linear relationship between F/L and $\sqrt{W}$ where F is the total force applied to each long edge, of intact length L. (Redrawn from [54].)

for shear, and

$$\frac{2Ea^3}{(3(1-\nu)(1+\nu))}, \tag{6}$$

for rotation.

2.3. Developing the local stiffness matrix

Consider two granules, sitting a distance L apart, in a two dimensional Cartesian coordinate system, with the local x axis passing through the nodes of both granules and the centre of the bond that is located half way between them. The granules are subjected to axial, shear and bending forces that are applied to the nodes of the lattice. Following the procedure presented by Livesley [53], the local stiffness matrix for the lattice member was constructed from an array of primitives:

$$\mathbf{P} = \begin{bmatrix} \frac{Ea}{(1-\nu^2)} & 0 & 0 \\ 0 & \frac{2Ea}{(2-\nu)(1+\nu)} & 0 \\ 0 & 0 & \frac{2Ea^3}{3(1-\nu)(1+\nu)} \end{bmatrix}, \tag{7}$$

based on the stiffnesses outlined in Section 2.2. Using the conventional approach of splitting the full stiffness matrix into four sub-matrices,

$$\mathbf{K} = \begin{bmatrix} k_{11} & k_{12} \\ k_{21} & k_{22} \end{bmatrix}, \tag{8}$$

and the full matrix, $\mathbf{K}$, can be obtained from the sub-matrices using

$$k_{ij} = \mathbf{H}_i \mathbf{P} \mathbf{H}_j^T, \tag{9}$$

where i and j can take the values 1 or 2, and

$$\mathbf{H}_1 = -\begin{bmatrix} 1 & 0 & 0 \\ 0 & 1 & 0 \\ 0 & L/2 & 1 \end{bmatrix}, \tag{10}$$

and

$$\mathbf{H}_2 = \begin{bmatrix} 1 & 0 & 0 \\ 0 & 1 & 0 \\ 0 & -L/2 & 1 \end{bmatrix}. \tag{11}$$

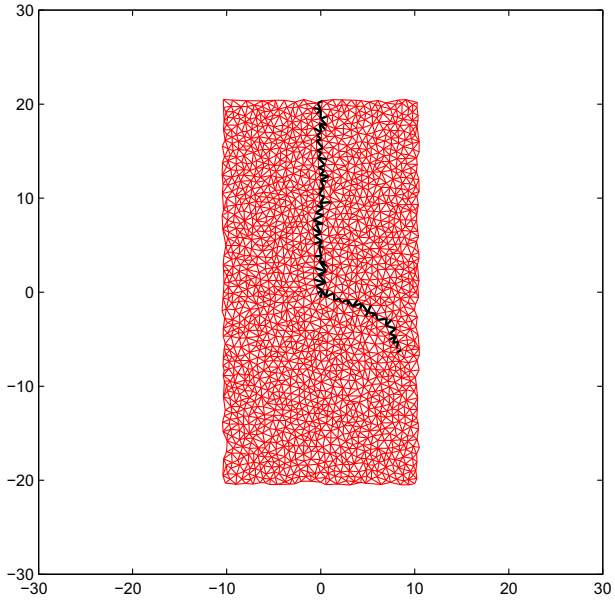

Fig. 6. Propagation of kinked crack. Cracks shown as thick black lines.

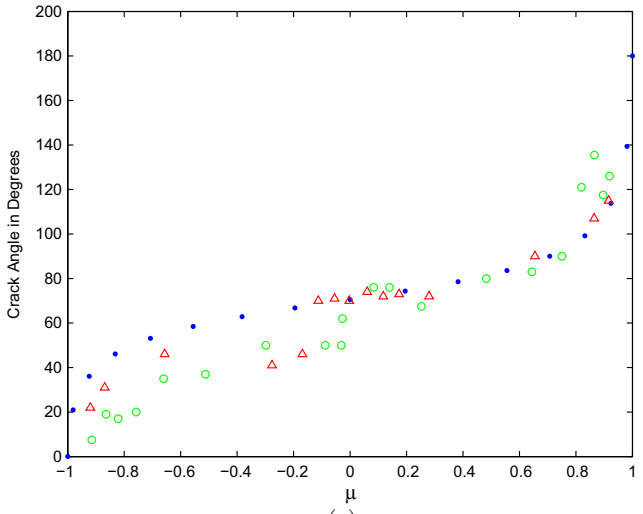

Fig. 7. Analysis of kinked crack. $\mu = \frac{\left(\frac{K_I}{K_{II}}\right)}{\sqrt{\left(\frac{K_I}{K_{II}}\right)^2 + 1}}$. Blue dots show the theoretical predictions. Predictions using the model (for two different assemblies) are shown as green circles and red triangles. (For interpretation of the references to colour in this figure legend, the reader is referred to the web version of this article.)

The stiffness matrix thus developed can then be used following the classic approach: **f** = **Ku**; where **f** is the vector of nodal forces; **K** is the stiffness matrix and **u** is the vector of nodal displacements.

3. Testing the model

3.1. Applying the boundary conditions

The boundary conditions were applied by selecting those boundary nodes that would be given prescribed displacements. The analysis proceeded in the conventional manner for a standard stiffness method problem and the loads at each bond were evaluated. All the simulations presented in this paper used prescribed displacements and did not proceed by applying loads to any of the nodes. The forces required to produce those deformations were calculated (when required) from the vector of nodal forces produced by the simulation. As the granule to granule connectivity was defined in terms of a 'beam like' stiffness matrix, granule rotation could be prescribed by applying a rotation to the relevant end of the appropriate 'beam'. It should be recalled that the simulations are comparative only as no specific material is being simulated.

3.2. Checking isotropic behaviour

It was necessary to ensure that a random array of bonded granules would produce an assembly that manifested an isotropic response. Such arrays were generated as described in Section 2.1 and the orientation of the bonds was checked by constructing polar histograms of the orientation of the elements that formed the Delaunay triangulations. The bonds to be examined were selected randomly using a Matlab algorithm and a large number of bonds were examined for several different granule arrays. Typical histograms are shown in Fig. 2. These checks demonstrated that the procedure outlined in Section 2 would produce a truly isotropic array.

3.3. Linear elastic behaviour

The inter-granular bonds obey Hooke's law. The constitutive relationships between stress, σ, and strain, ε, for a two dimensional system are shown below.

$$\varepsilon_{xx} = \frac{\sigma_{xx}}{E} - \frac{\nu\sigma_{yy}}{E}, \tag{12}$$

$$\varepsilon_{yy} = \frac{\sigma_{yy}}{E} - \frac{\nu\sigma_{xx}}{E}, \tag{13}$$

$$\varepsilon_{xy} = \frac{\sigma_{xy}}{2G}, \tag{14}$$

where the subscripts relate to the x and y axes in the usual manner.

The mechanical response of granular assemblies constructed as described in Section 2 has been reported [54] to be consistent with a 2D isotropic linear elastic solid.

3.4. Simulating fracture

The work described in the previous section indicated that initially the bulk behaviour of the assembly was isotropic. The bond between two adjacent grains was assumed to occur at the midpoint of the lattice member joining the nodes representing each grain. It follows that the bond stresses were not uniform. The area of the contact between two grains was assumed to be small compared to the size of the grain. It can be seen from Section 2.2 that the size of the contact has much greater influence on the bending stiffness than on the shear or axial stiffness.

Fracture was simulated as follows. First the displacements at the support points were constrained to provide appropriate boundary conditions. An appropriate point, or set of points, P, on the body was given a set displacement, U_{set}, and the reactions (F) determined. The bond tensions, T, were determined and used to calculate $\lambda = T/S$ (where S is the bond strength) for each bond. The bond with the maximum value of λ (denoted as λ_n^{max}, where n related to the simulation step) was then recorded as being broken and its stiffness subtracted from the appropriate elements of the stiffness matrix. F_n and λ_n^{max} were stored and the modified lattice re-analysed and the process repeated. Clearly the stiffness of the body being simulated reduced with each fracture. The simulation continued until the body was deemed to have completely failed.

The load versus displacement plots were then created. Prior to loading the displacement was zero, and the displacement associated with the first fracture, $\lambda_1^{max} U_{set}$, was plotted against the value

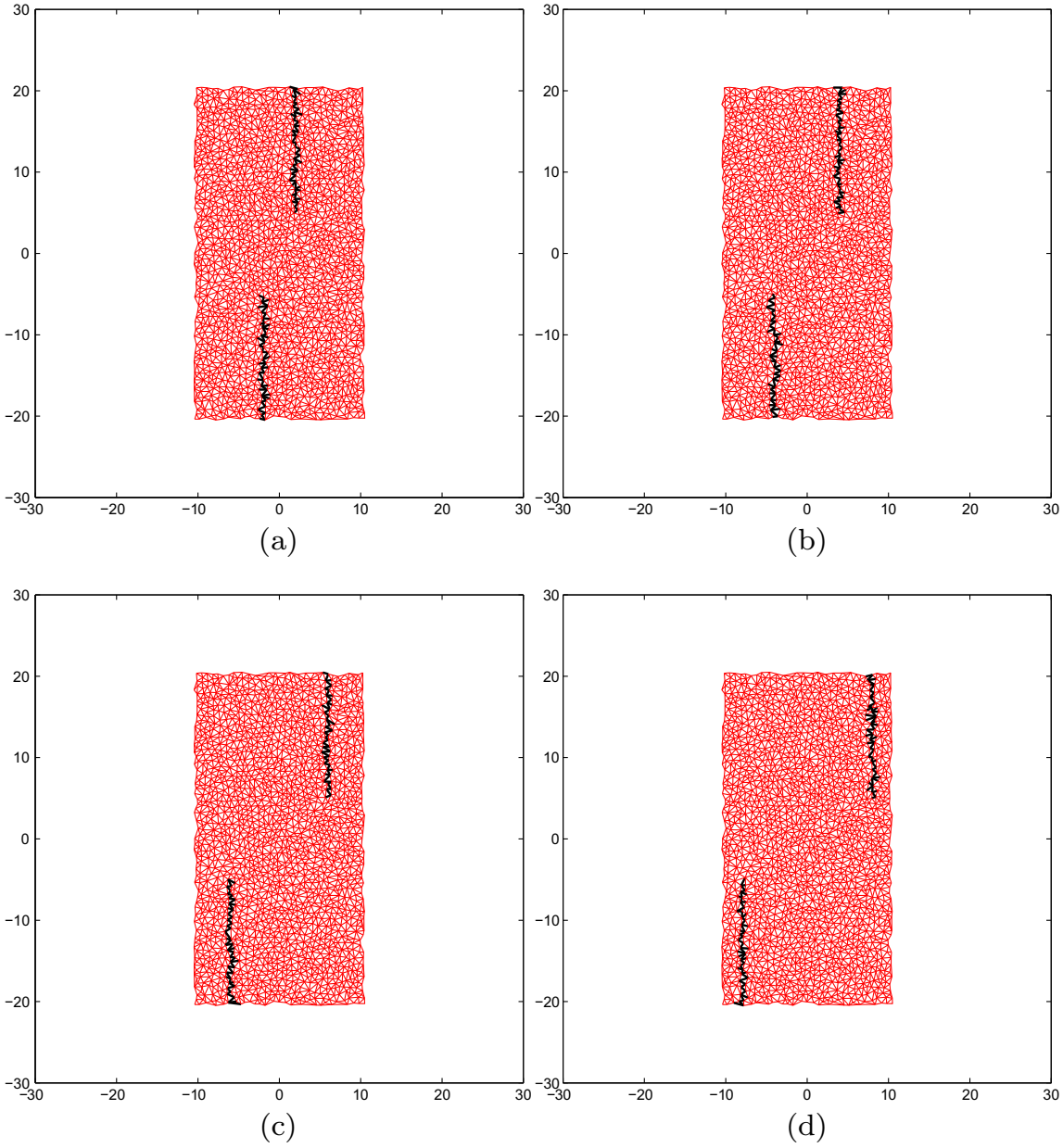

Fig. 8. Arrangement of opposing off-set pre-cracks. Cracks shown as thick black lines.

of $\lambda_1^{max}F_1$, with the slope of the plot equivalent to the initial stiffness of the undamaged body. Fractures that occur red in the simulation after that first fracture sometimes produced values of $\lambda_n^{max}U_{set}$ that were smaller than $\lambda_1^{max}U_{set}$. These were part of an unstable fracture process initiated by the first fracture. The next fracture for which the value of λ_n^{max} exceeded the previous maximum was then established and $\lambda_n^{max}F_n$ versus $\lambda_n^{max}U_{set}$ plotted, ignoring any unstable fractures. The 'step' changes in the stiffness of the body as fracture progressed are evident in the plots shown in Figs. 11, 13 and 14 and illustrate are the tension softening known to occur in materials of the type being simulated in the work presented here.

3.5. Propagation of a straight crack

A standard crack test was simulated by first constructing a rectangular assembly of randomly distributed granules. A small section of bonds located at the mid-width and near the top of the assembly were removed from consideration in the loading algorithm, as illustrated in Fig. 3. The elements removed have been shown as a thick black line for clarity. The boundary nodes were prevented from moving vertically, and the boundary nodes at either side were displaced horizontally outwards to encourage the pre-existing crack to grow. The crack extension predicted by the model is as expected and is shown in Fig. 4, on the un-deformed geometry.

An examination of the bond forces during the simulations revealed much higher forces in the bonds at the crack tip, consistent with the expected stress concentration at this position, and near uniform strain in the uncracked portion. Results of dimensional analysis predict that, for the test described above carried out on a sample of width W, a relationship exists between the total force (F) applied to each long edge, of intact length, L, such that $\sqrt{W}$ is proportional to F/L. A large number of tests were carried out [54] using the model presented here for samples of various widths (W) and the results are illustrated in Fig. 5. This confirms the linear relationship between F/L and $\sqrt{W}$.

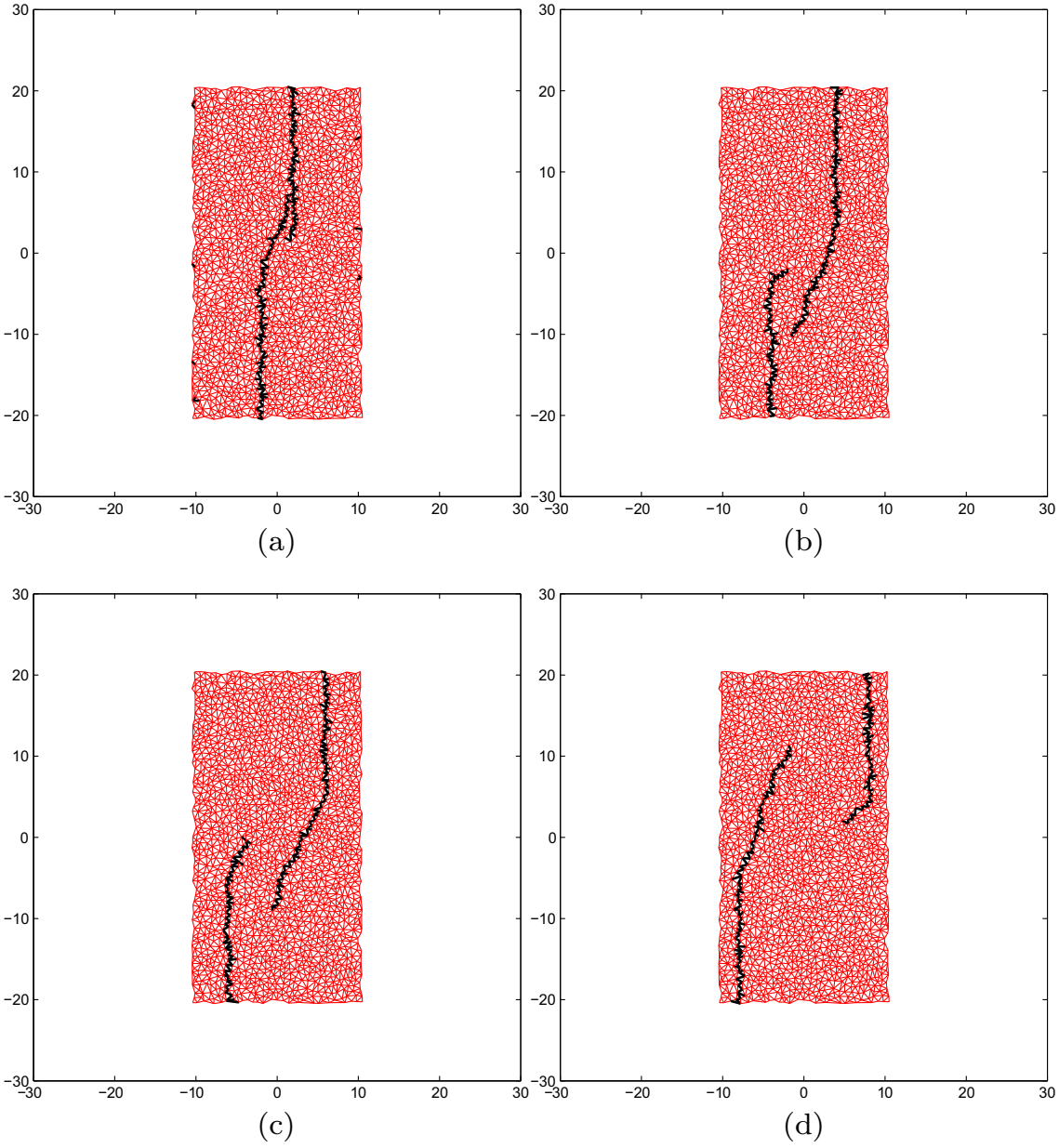

Fig. 9. Propagation of opposing off-set pre-cracks shown in Fig. 8. Cracks shown as thick black lines.

3.6. Propagation of a kinked crack

The behaviour of the model when propagating a kinked crack was investigated by setting up a sample, pre-cracked for a set length, generally as indicated in Fig. 3. For this test the nodes on the right hand vertical boundary of the assembly were displaced outwards and upwards, while those on the left hand vertical boundary were displaced outwards and downwards, but were free to rotate. All the other nodes were free to displace and rotate in response to the displacement of the boundary nodes. The resulting crack propagation is shown in Fig. 6. This test simulates Mode II cracking in the kinked portion of the crack (i.e. ignoring the section that was pre-cracked before the application of any load).

Classic fracture mechanics [55] provides the following relationship

$$\sigma_\theta = \frac{1}{(2r)^{\frac{1}{2}}} \cos\frac{\theta}{2}\left[K_I \cos^2\frac{\theta}{2} - \frac{3}{2}K_{II}\sin\theta\right], \tag{15}$$

where σ_θ is the hoop stress at an angle θ from the pre-existing crack and a distance r from the crack tip; and K_I and K_{II} are the stress intensity factors for Mode I and Mode II loading respectively. A large number of simulations were then carried out for a particular granular arrangement containing a crack as shown in Fig. 3. The assembly was then subjected to a variety of deformations consisting of a combination of horizontal and vertical displacement of the two vertical boundaries. This pattern of deformation produced kinked cracks of the form shown in Fig. 6. The angle that the kinked portion of the crack made with the vertical drawn through the initial crack was measured from the plotted figures showing crack growth. The values of K_I and K_{II} were calculated from the following formulae,

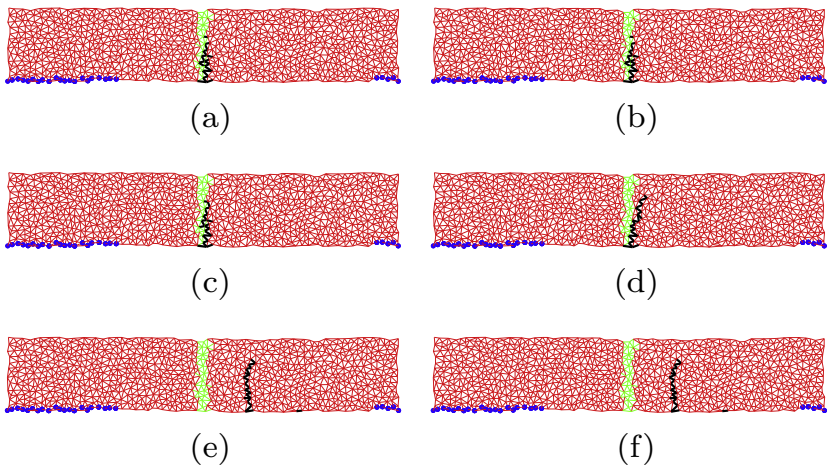

Fig. 10. Idealised Schematic of Masonry (shown red) with central mortar (shown green) loaded by displacing the upper surface downwards to mimic a UDL on the upper surface and supported as indicated by blue dots. It should be noted that the supports are not symmetrical and so the maximum moment does not occur at the mid-point of the beam. Cracks shown as thick black lines. (a) Mortar strength at 10% of masonry strength; (b) mortar strength at 20% of masonry strength; (c) mortar strength at 40% of masonry strength; (d) mortar strength at 60% of masonry strength; (e) mortar strength at 80% of masonry strength; (f) mortar strength at 100% of masonry strength. (For interpretation of the references to colour in this figure legend, the reader is referred to the web version of this article.)

derived using the procedure presented by Rice in a discussion [56] on a paper by Knauss [57].

$$K_I = \sigma_{11}(1-\nu)^{\frac{1}{2}}h_w^{\frac{1}{2}}, \tag{16}$$

and

$$K_{II} = (1+\nu)^{\frac{1}{2}}\sigma_{12}(2h_w)^{\frac{1}{2}}, \tag{17}$$

where σ_{11} is the stress at the crack tip that tends to open the crack in Mode I, σ_{12} is the shear stress at the crack tip, ν is Poisson's ratio (taken as 0.19 for these simulations, following work by Adaiem [54]) and h_w is half the width of the sample. This permitted a parameter μ to be determined

$$\mu = \frac{\left(\frac{K_I}{K_{II}}\right)}{\sqrt{\left(\frac{K_I}{K_{II}}\right)^2 + 1}}. \tag{18}$$

The values of K_I and K_{II} were determined as outlined above, from the boundary reactions, during the first loading run of the simulation (i.e. at the onset of crack propagation). This was repeated for each deformation arrangement (i.e. for a range of values of μ) and for two different assemblies. The results obtained from the simulations are compared with the theory in Fig. 7.

It is clear from Fig. 7 that, as one would expect, the model behaviour is influenced by the granular arrangement and the significance of this was investigated by running simulations using different randomly created granular arrangements for the same deformation mechanism. Deformation mechanisms associated with $\frac{K_I}{K_{II}} = 0.0$ and $\frac{K_I}{K_{II}} = 1.0$ were explored and ten assemblies created for each mechanism. The first of these produced (for the first deformation mechanism) an average $\frac{K_I}{K_{II}} = -0.0250$ and a variance of 0.0064, while the second produced (for the second deformation mechanism) an average $\frac{K_I}{K_{II}} = 0.9499$ and a variance of 0.0024. A third set of randomly generated assemblies was created using a denser packing mechanism and evaluated using the second deformation mechanism. This resulted in an average $\frac{K_I}{K_{II}} = 0.9799$ and a variance of 0.0012. The procedure was then repeated (again for the second deformation mechanism), in an attempt to place more granules within the sample boundaries in order to achieve a greater packing density. This produced an average $\frac{K_I}{K_{II}} = 0.9421$ and a variance of 0.0022. Clearly, the number of granules that can be placed within a set boundary depends on the limit placed on the minimum granule size and these results suggest that the initial simulations were close to the optimum for the granule size chosen.

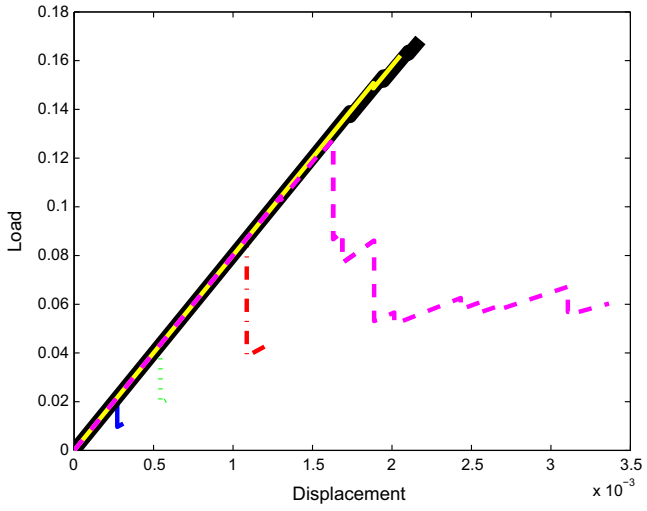

Fig. 11. Load versus displacement curves for the simulations shown in Fig. 10. The short, solid blue line relates to a mortar strength at 10% of the masonry strength; the doted green line relates to a mortar strength at 20% of the masonry strength; the red dash-dot line relates to a mortar strength at 40% of the masonry strength; the dashed magenta line relates to mortar strength at 60% of the masonry strength (this simulation was run for a greater number of increments than the others to show the full crack development); the solid thick black line relates to a mortar strength at 80% of the masonry strength; the thin yellow line relates to a mortar strength at 100% of the masonry strength. The simulations to which this figure relates were conducted for comparison purposes only and did not relate to any specific material. It follows that the numerical values shown for the load and the displacement are not significant. The grain size is, on average, about 1.2% of the length of the wall, and the area of the contacts bonding the grains is, on average, about 1.9% of the surface area of the each of the grains that it connects. (For interpretation of the references to colour in this figure legend, the reader is referred to the web version of this article.)

These tests indicate that the model captures the essential features of linear elastic fracture mechanics and can simulate the behaviour of real, weakly bonded granular assemblies (such as

Fig. 12. Idealised schematic of a flat arch restrained at the ends from moving outwards or downwards and loaded by vertically displacing two nodes on the upper surface to mimic a small patch of distributed load. The mortar (shown green) strength is 10% of the masonry (shown red) strength. Cracks shown as thick black lines. (For interpretation of the references to colour in this figure legend, the reader is referred to the web version of this article.)

sedimentary rocks, lean mix concrete and concrete formed using strong aggregate, and several types of ceramic formed from strong grains – such as grinding wheels).

4. Predictions using the model

4.1. Propagation of two opposing off-set cracks

The model was then used to explore the response of two opposing cracks, off-set from each other, when the bond strength is uniform. Four arrangements of pre-cracks were examined, as shown in Fig. 8. In each case the cracks were propagated by displacing the vertical boundaries of the cracked body outwards. In this manner simple tension was simulated, with no shear element. The propagation of the cracks is shown in Fig. 9 and generally follows the pattern found experimentally by Fender et al. [39] and Cortet et al. [38].

4.2. Exploring the settlement of masonry

Simulations of a simplified schematic of a masonry wall were carried out on a geometry shown in Fig. 10. The masonry units are indicated in red and the central mortar joint between them is shown in green. The upper surface was displaced downwards to mimic a downward acting uniformly distributed load (UDL), and the support to the central portion was removed leaving supports only at the ends, as indicated by the blue dots. The strength of the elements in the mortar were set to different fractions of those in the masonry units. It should be noted that the supports are not symmetrical so the maximum bending moment does not coincide with the position of the mortar joint.

Fig. 10(a–f) shows that, when the mortar strength is much lower than the that of the masonry, the crack is confined to the mortar joint; but as the strength of the mortar increases, the crack first starts to diverge from its initiation point within the mortar into the masonry (see Fig. 10(d)) and, as the strength increases again, the crack position moves to a point determined by the geometry and uninfluenced by the relative strengths. The tendency of the crack to curve as it extends into the masonry unit is noted and conforms to observations [36,58]. The simulation shown in Fig. 10(d) was allowed to run for a greater number of increments than the others to show the tension softening of the material as is illustrated in Fig. 11.

4.3. Exploring the behaviour of a flat arch

A simulation of a flat arch was carried out as illustrated in Fig. 12. Motion of the nodes on the two vertical boundaries was prevented, and two nodes the upper surface near mid-span were displaced downwards to mimic a central patch load. The strength of the mortar was kept at 10% of the masonry strength and, as can be seen, the cracks occur in the tension zones and are mainly confined to the mortar joints. As the cracks develop they show the tendency to curve that has been considered earlier.

4.4. Simulating standard tests

A diametrical compression test (or cylinder splitting test) was simulated using the model and produced the classic crack pattern as shown in Fig. 13(a). The load vs displacement curve produced by this simulation is shown in Fig. 13(b). It should be recalled that the simulation does not relate to any specific material and so the numerical values are not significant and serve only to aid comparison. The curve clearly shows the strain softening, known to occur post-peak load in brittle materials of the type being considered.

A four point bend test was simulated as shown in Fig. 14(a). The two nodes on the upper surface indicated by the blue circles were displaced vertically downwards while the two nodes on the lower surface indicated by the green circles were prevented from moving

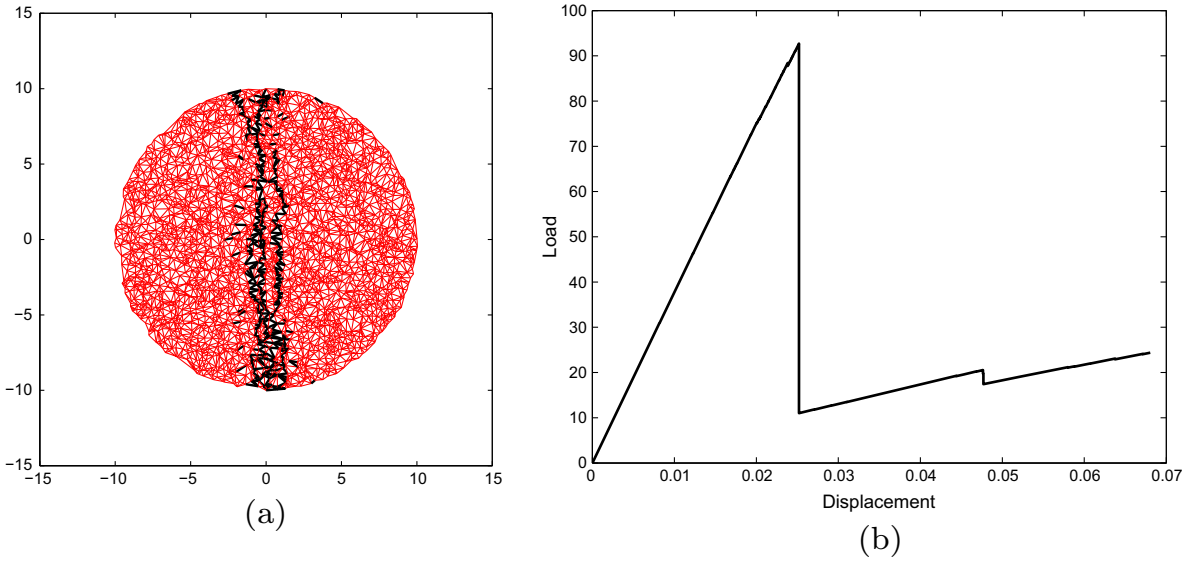

Fig. 13. Diametrical compression test. (a) Cracked cylinder after loading. (b) Load vs displacement curve. This simulation does not relate to any specific material and so the numerical values shown for the load and the displacement are not significant. The grain size is, on average, about 1.8% of the diameter of the cylinder, and the area of the contacts bonding the grains is, on average, about 1.85% of the surface area of the each of the grains that it connects.

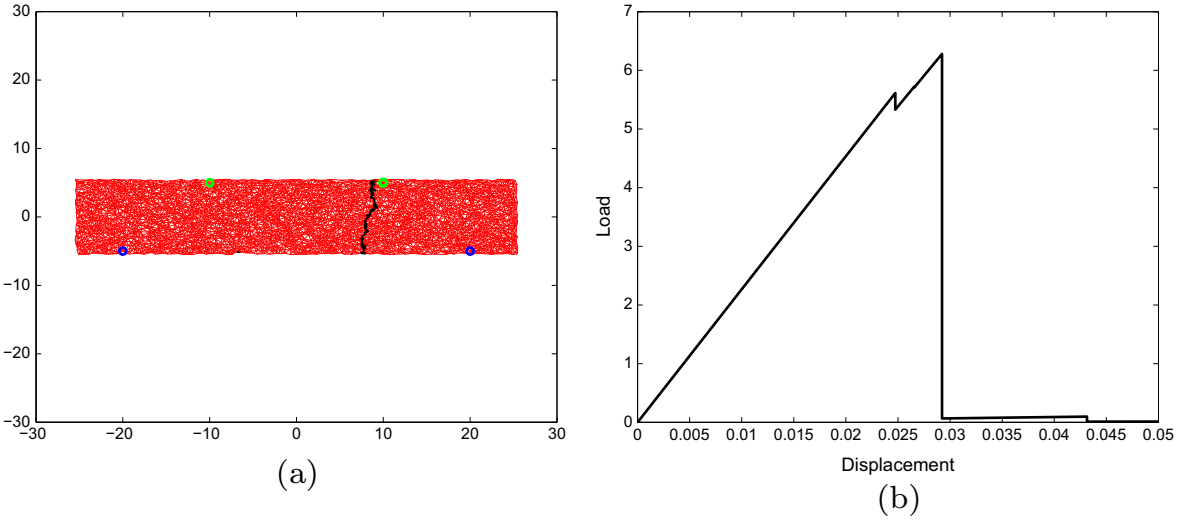

Fig. 14. Four point bend test. Downwards point loads applied (by means of fixed displacements) on the upper surface at the positions indicated by the blue circles. Vertical displacement was prevented at the positions on the lower surface indicated by the two green circles and horizontal displacement was prevented at the green circle on the right hand side. (a) Cracked beam after loading. (b) Load vs displacement curve. This simulation does not relate to any specific material and so the numerical values shown for the load and the displacement are not significant. The grain size is, on average, about 0.8% of the length of the beam, and the area of the contacts bonding the grains is, on average, about 0.06% of the surface area of the each of the grains that it connects. (For interpretation of the references to colour in this figure legend, the reader is referred to the web version of this article.)

vertically. Two simulations were run, horizontally restraining each of the lower nodes in turn, but there was no noticeable difference in the results. The load vs displacement curve produced by this simulation is shown in Fig. 14(b). As before this does not relate to any specific material. The plot clearly shows the expected strain softening.

5. Concluding remarks

This paper presents a two dimensional lattice model that could easily be extended into three dimensions and that captures the essential behaviour of weakly bonded granular materials. In the context of this paper, 'weakly bonded' refers to the situation where fracture of the material would occur only by rupture of the inter-granule bonds, leaving the granules substantially intact. It has been demonstrated (see Figs. 5 and 7) that the model obeys the fundamental laws of linear elastic fracture mechanics. Inter-granule bond stiffnesses that more closely mimic the interaction between bonded granules than the more commonly assumed springs, bars or Euler–Bernoulli beams have been used to produce realistic simulations of the response of some brittle materials to load.

It is clear (see Fig. 2) that the model can satisfactorily simulate an isotropic material and it is clear from Section 4.2 that anisotropy could be introduced. Simulations conducted using the model confirm the experimentally observed behaviour that, in bonded granular materials, crack branching and crack merging rarely happen as a consequence of statically applied load. The tendency of off-set opposing cracks to 'bypass' each other, which has been observed by others [39,38], is confirmed by simulations presented here.

Simulations of an idealised portion of masonry with non-symmetric supports and subjected to load illustrates the significance of the relative strengths of the mortar compared to the masonry units and the influence of that on the resulting crack pattern. These simulations indicate that the model presented here, although developed to investigate cracking confined to the bonds between granules, could also be used to investigate through granule cracking. A clear understanding of the features of bonded granular materials that control cracking is very important for many engineering activities, including construction, tunnelling, drilling, hydraulic fracturing and mechanical forming. The tests and simulations presented here illustrate the utility of the model presented in this paper for investigating cracking in bonded granular assemblies.

References

[1] Chiaia B, Vervuurt A, van Mier JGM. Lattice model evaluation of progressive failure in disordered particle composites. Eng Fract Mech 1997;57(2/3):301–18.
[2] Raghuprasad BK, Bhat DN, Bhattacharya GS. Simulation of fracture in a quasi-brittle material in direct tension – a lattice model. Eng Fract Mech 1998;61:445–60.
[3] Topin V, Delenne JY, Radja F, Brendel L, Mabille F. Strength and failure of cemented granular matter. Eur Phys J E 2007;23:413–29.
[4] Kruyt NP, Rothenburg L. Micromechanical bounds for the effective elastic moduli of granular materials. Int J Solids Struct 2002;39:311–24.
[5] Zhao G-F, Russell AR, Zhao X, Khalili N. Strain rate dependency of uniaxial tensile strength in Gosford sandstone by the distinct lattice spring model with X-ray micro CT. Int J Solids Struct 2014;51:1587–600.
[6] Katsman R, Aharonov E, Scher H. Numerical simulation of compaction bands in high-porosity sedimentary rock. Mech Mater 2005;37:143–62.
[7] Katsman R, Aharonov E. A study of compaction bands originating from cracks, notches, and compacted defects. J Struct Geol 2006;28:508–18.
[8] Potyondy DO, Cundall PA. A bonded-particle model for rock. Int J Rock Mech Min Sci 2004;41:1329–64.
[9] Schlangen E, Garboczi EJ. Fracture simulations of concrete using lattice models: computational aspects. Eng Fract Mech 1997;57:319–32.
[10] Ince R, Arslan A, Karihaloo BL. Lattice modelling of size effect in concrete strength. Eng Fract Mech 2003;70(16):2307–20.
[11] Savija B, Lukovic M, Pacheco J, Schlangen E. Cracking of the concrete cover due to reinforcement corrosion: a two-dimensional lattice model study. Constr Build Mater 2013;44:626–38.
[12] Savija B, Lukovic M, Pacheco J, Schlangen E. Lattice modeling of chloride diffusion in sound and cracked concrete. Cem Concr Compos 2013;42:30–40.
[13] Lilliu G, van Mier JGM. 3d lattice type fracture model for concrete. Eng Fract Mech 2003;70:927–41.
[14] Chandler HW. Thermal stress in ceramics. Trans J Br Ceram Soc 1981;80:191–5.
[15] Affes R, Delenne JY, Onerie Y, Radje F, Topin V. Tensile strength and fracture of cemented granular aggregates. Eur Phys J E 2012;35:117–32.
[16] Berton S, Bolander JE. Crack band model of fracture in irregular lattices. Comput Methods Appl Mech Eng 2006;192:7172–81.
[17] Schlangen E, Garboczi EJ. New method for simulating fracture using an elastically uniform random geometry lattice. Int J Eng Sci 1996;34:1131–44.
[18] Ostoja-Starzewski M, Sheng PY, Alzebdeh K. Spring network models in elasticity and fracture of composites and polycrystals. Comput Mater Sci 1996;7:82–93.

[19] Ibrahimbegovic A, Delaplace A. Microscale and mesoscale discrete models for dynamic fracture of structures built of brittle material. Comput Struct 2003;81:1255–65.
[20] Karihaloo BL, Carpinteri A, Elices M. Fracture mechanics of cement mortar and plain concrete. Adv Cem Based Mater 1993;1:92–105.
[21] Pchenik L, Levine H, Kessler D. Steady-state mode I cracking in a viscoelastic triangular lattice. J Mech Phys Solids 2002;50:583–613.
[22] Heizler SI, Kessler DA, Levine H. Propagating mode-I fracture in amorphous materials using the continuous random network model. Phys Rev E 2011;84(2) [Article 026102 Part 2].
[23] Kim K, Bolander JE, Lim YM. Failure simulation of RC structures under highly dynamic conditions using random lattice models. Comput Struct 2013;125:127–36.
[24] Yip M, Li Z, Liao BS, Bolander JE. Irregular lattice models of fracture of multiphase particulate materials. Int J Fract 2006;140:113–24.
[25] Cho N, Martin CD, Sego DC. A clumped particle model for rock. Int J Rock Mech Min Sci 2007;44:997–1010.
[26] Mair K, Abe S. Breaking up: comminution mechanisms in sheared simulated fault gouge. Pure Appl Geophys 2011;168:2277–88.
[27] Elias J, Stang H. Lattice modeling of aggregate interlocking in concrete. Int J Fract 2012;175:1–11. http://dx.doi.org/10.1007/s10704-012-9677-3.
[28] Thornton C, Barnes DJ. Computer simulated deformation of compact granular assemblies. Acta Mech 1986;64(1):45–61.
[29] Ouadfel H, Rothenburg L. Stress-force fabric relationship for assemblies of ellipsoids. Mech Mater 2001;33:201–21.
[30] Kruyt NP, Agnolin I, Luding S, Rothenburg L. Micromechanical study of elastic moduli of loose granular materials. J Mech Phys Solids 2010;58:1286–301.
[31] Andre D, Jebahi M, Charle J-L, Néauport J. Using the discrete element method to simulate brittle fracture in the indentation of a silica glass with a blunt indenter. Comput Methods Appl Mech Eng 2013;263:136–47.
[32] Sands CM, Henderson RJ, Chandler HW. A three dimensional computational model of the mechanical response of a dual-phase ceramic. Comput Mater Sci 2007;39:862–70.
[33] Liu HY, Roquette M, Kou SQ, Lindqvist P-A. Characterization of rock heterogeneity and numerical verification. Eng Geol 2004;72:89–119.
[34] Li L, Meng Q, Wang S. A numerical investigation of the hydraulic fracturing behaviour of conglomerate in Glutenite formation. Acta Geomech 2013;8:597–618.
[35] Wang SY, Sloan SW, Liu HY, Tang CA. Numerical simulation of the rock fragmentation process induced by two drill bits subjected to static and dynamic (impact) loading. Rock Mech Eng 2011;44:317–32.
[36] Erdogan F, Sih GC. On the crack extension in plates under plain loading and transverse shear. Trans Am Soc Mech Eng, J Basic Eng 1963;85:519–27.
[37] Melin S. Why do cracks avoid each other? Int J Fract 1983;23(1):37–45.
[38] Cortet P-P, Huillard G, Vanel L, Ciliberto S. Attractive and repulsive cracks in a heterogeneous material. J Stat Mech: Theory Exp 2008 [Article P10022].
[39] Fender ML, Lechenault F, Daniels KE. Universal shapes formed by two interacting cracks. Phys Rev Lett 2010;105(12) [Article 125505].
[40] Pande GN, Liang JX, Middleton J. Equivalent elastic moduli for brick masonry. Comput Geotech 1989;8:243–65.
[41] Lee JS, Pande GN, Middleton J, Kralj B. Numerical modelling of brick masonry panels. Comput Struct 1996;61(4):735–45.
[42] Alpa G, Monetto I. Microstructural model for dry block masonry walls with in-plane loading. J Mech Phys Solids 1994;42(7):1159–75.
[43] Anthoine A. Derivation of the in-plane elastic characteristics of masonry through homogenization theory. Int J Solids Struct 1995;32(2):137–63.
[44] Luciano R, Sacco E. Homogenization technique and damage model for old masonry material. Int J Solids Struct 1997;34(24):3191–208.
[45] Sab K. Yield design of thin periodic plates by a homogenization technique and an application to masonry walls. CR Mec 2003;331:642–6.
[46] Cecchi A, Sab K. A comparison between a 3d discrete model and two homogenised plate models for periodic elastic brickwork. Int J Solids Struct 2004;41:2259–76.
[47] Cecchi A, Sab K. A homogenized Love–Kirchhoff model for out-of-plane loaded random 2d lattices: application to "quasi-periodic" brickwork panels. Int J Solids Struct 2009;46:2907–19.
[48] Milani G. Simple lower bound limit analysis homogenization model for in-and-out-of-plane loaded masonry walls. Constr Build Mater 2011;25:4426–43.
[49] Hammoud M, Sab K, Duhamel D. A coupled discrete/continuous method for computing lattices. Application to masonry-like structure. Int J Solids Struct 2011;48(21):3091–8.
[50] Casolo S, Milani G. A simplified homogenization-discrete element model for the non-linear static analysis of masonry walls out-of-plane loaded. Eng Struct 2010;32(8):2352–66.
[51] Barber JR. Elasticity (solid mechanics and its application). Springer; 1992.
[52] Johnson KL. Contact mechanics. paperback ed. Cambridge: Cambridge University Press; 1987 [section 7.2].
[53] Livesley RK. Matrix methods of structural analysis. Oxford: Pergamon Press; 1975.
[54] Adaiem MH. Wellbore integrity in shale strata. PhD thesis. University of Aberdeen; 2010.
[55] Williams ML. On the stress distribution at the base of a stationary crack. J Appl Mech 1957;24:109–14.
[56] Rice JR. Discussion on stresses in an infinite strip containing a semi-infinite crack. Trans Am Soc Mech Eng 1967:248–9.
[57] Knauss WG. Stresses in an infinite strip containing a semi-infinite crack. ASME J Appl Mech 1966;33:356–62.
[58] Cotterell B, Rice JR. Slightly curved or kinked cracks. Int J Fract 1980;16(2):155–69.